



Extreme Variability in a Long-duration Gamma-Ray Burst Associated with a Kilonova

P. Veres^{1,2}, P. N. Bhat², E. Burns³, R. Hamburg⁴, N. Fraija⁵, D. Kocevski⁶, R. Preece², S. Poolakkil^{1,2}, N. Christensen⁷, M. A. Bizouard⁷, T. Dal Canton⁴, S. Bala⁸, E. Bissaldi^{9,10}, M. S. Briggs^{1,2}, W. Cleveland⁸, A. Goldstein⁸, B. A. Hristov², C. M. Hui¹¹, S. Lesage^{1,2}, B. Mailyan¹², O. J. Roberts¹³, and C. A. Wilson-Hodge¹¹

¹Department of Space Science, University of Alabama in Huntsville, Huntsville, AL 35899, USA; peter.veres@uah.edu

²Center for Space Plasma and Aeronomic Research, University of Alabama in Huntsville, Huntsville, AL 35899, USA

³Department of Physics & Astronomy, Louisiana State University, Baton Rouge, LA 70803, USA

⁴Université Paris-Saclay, CNRS/IN2P3, IJCLab, F-91405 Orsay, France

⁵Instituto de Astronomía, Universidad Nacional Autónoma de México, Circuito Exterior, C.U., A. Postal 70-264, 04510, CDMX, Mexico

⁶NASA Marshall Space Flight Center, Martin Rd. SW, Huntsville, 35808, AL, USA

⁷Université Côte d'Azur, Observatoire de la Côte d'Azur, CNRS, Artemis, F-06300 Nice, France

⁸Science and Technology Institute, Universities Space Research Association, Huntsville, AL 35805, USA

⁹Dipartimento Interateneo di Fisica, Politecnico di Bari, Via E. Orabona 4, I-70125 Bari, Italy

¹⁰INFN—Sezione di Bari, Via E. Orabona 4, I-70125 Bari, Italy

¹¹ST12 Astrophysics Branch, NASA Marshall Space Flight Center, Huntsville, AL 35812, USA

¹²Department of Aerospace, Physics and Space Sciences, Florida Institute of Technology, Melbourne, FL 32901, USA

¹³Science and Technology Institute, Universities Space and Research Association, 320 Sparkman Drive, Huntsville, AL 35805, USA

Received 2023 May 22; revised 2023 July 10; accepted 2023 July 12; published 2023 August 24

Abstract

The recent discovery of a kilonova from the long-duration gamma-ray burst (GRB) GRB 211211A challenges classification schemes based on temporal information alone. Gamma-ray properties of GRB 211211A reveal an extreme event, which stands out among both short and long GRBs. We find very short variations (few milliseconds) in the lightcurve of GRB 211211A and estimate ~ 1000 for the Lorentz factor of the outflow. We discuss the relevance of the short variations in identifying similar long GRBs resulting from compact mergers. Our findings indicate that in future gravitational-wave follow-up campaigns, some long-duration GRBs should be treated as possible strong gravitational-wave counterparts.

Unified Astronomy Thesaurus concepts: [Gamma-ray bursts \(629\)](#); [Gamma-rays \(637\)](#)

Supporting material: machine-readable table

1. Introduction

Gamma-ray bursts (GRBs) are typically classified into long or short groups based on the duration of the active gamma-ray episode. Such a classification has historical origins (Kouveliotou et al. 1993), and the physical understanding behind this picture has matured over the following decades: short GRBs (sGRBs) are predominantly from binary neutron star mergers (Duncan & Thompson 1992; Usov 1992; Thompson 1994; Abbott et al. 2017; Goldstein et al. 2017) or possibly from black hole–neutron star mergers (Narayan et al. 1992), while long GRBs (IGRBs) originate from the core collapse of massive stars (Woosley 1993; Paczyński 1998; MacFadyen & Woosley 1999; Woosley & Bloom 2006). There is an overlap between the duration distributions of short and long classes. For this reason, the classification based on the burst duration is complemented by rudimentary spectral information, the hardness ratio (HR), available for all GRBs. Classifications based on two parameters provide better separation between the classes. On average, sGRBs are harder, while IGRBs are softer (Paciesas et al. 1999; Bhat et al. 2016; von Kienlin et al. 2020). In some cases even two parameters are not sufficient to derive a reliable classification and further observations are needed to hone in on the physical origin of the GRBs (see, e.g., the Type I/II classification scheme by

Zhang et al. 2009 and refer to Kann et al. 2011 for a discussion of controversial scenarios). IGRBs also include ultralong GRBs (ULGRBs) with a duration longer than thousands of seconds (Gendre et al. 2013; Levan et al. 2014; Piro et al. 2014; Greiner et al. 2015; Kann et al. 2018), and IGRBs associated with Type Ic supernovae (SNe Ic; Hjorth et al. 2003). Additionally giant flares from extragalactic magnetars (Roberts et al. 2021) can masquerade as sGRBs at a rate of approximately one event per year (Burns et al. 2021), further complicating the picture.

At first glance, GRB 211211A is a bright, but otherwise typical IGRB suggesting a collapsar origin, based on the gamma-ray properties. However, Rastinejad et al. (2022) and Troja et al. (2022) report a possible kilonova counterpart to GRB 211211A suggesting a compact merger origin, at odds with the gamma-ray classification. GRB 211211A represents one of the clearest breaks with the usual short/long classification. Some sGRB pulses are followed by a longer, extended gamma-ray emission, without associated supernovae. Furthermore the initial pulse's spectral lag and luminosity are consistent with sGRBs, even if their duration is somewhat over the canonical 2 s limit. This is the case for the GRB 060614 (Gehrels et al. 2006), which was classified as a potential member of the sGRB with extended emission class by Lien et al. (2016). It is possible that GRB 211211A also belongs to this class.

One of the most intriguing features of GRBs is the short variations in their lightcurves (see, e.g., Camisasca et al. 2023 for a recent study). The observed variability could originate from the variations in the central engine with contributions

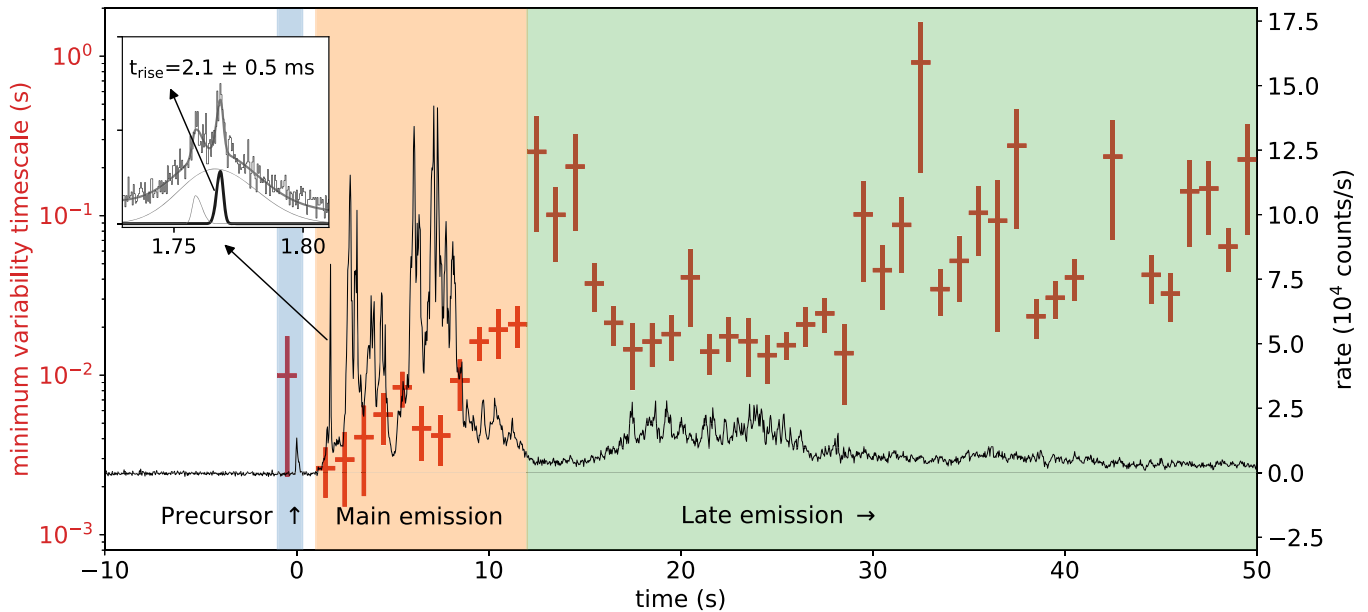


Figure 1. Lightcurve of GRB 211211A (black) and the corresponding minimum variability timescale (red). Inset: zoomed lightcurve around the time of the shortest variation. Individual pulse models are indicated, with the shortest rise time highlighted in bold.

from the jet interacting with the progenitor (Sari & Piran 1997a; Morsony et al. 2010). This variability is imprinted on the emission processes (e.g., internal shocks; Sari & Piran 1997b), or alternatively can be ascribed to intrinsic variations in the emitting volume (e.g., by turbulence; Narayan & Kumar 2009). Typical variations can be as short as 10 ms, with a handful of examples of sub-10 ms variability. The most extreme case for a GRB is a $\sim 200 \mu\text{s}$ variation (Bhat et al. 1992). On average, sGRBs have shorter variability than IGRBs (Bhat et al. 2012; Golkhou et al. 2015). The variability timescale constrains the size of the emitting region based on causality arguments (Rybicki & Lightman 1979).

Here, we place GRB 211211A in the context of Fermi Gamma-ray Burst Monitor (GBM) GRBs and report on the implications for future gravitational-wave (GW) or kilonova searches associated with GRBs. We provide a detailed analysis of the gamma-ray lightcurve highlighting the extreme variability and discuss the possible association of this GRB with the class of sGRBs with extended emission.

We present gamma-ray observations of GRB 211211A in Section 2, focusing on the minimum variability timescale (Section 3). We present GRB 211211A as a GRB with extended emission and provide physical parameters of the outflow in Section 4. We end with discussing our results in Section 5. We use the $Q_x = Q/10^x$ convention in c.g.s. units for quantity Q and refer to physical constants using their common notations.

2. Data Analysis

GRB 211211A (Mangan et al. 2021) triggered Fermi-GBM (Meegan et al. 2009) at 13:09:59.65 UT on 2021 December 11, (T_0). It showed significant emission in all 12 of GBM’s NaI and both the Bismuth Germanate (BGO) detectors, up to an energy ~ 20 MeV. At trigger time the location of the GRB was outside of the Large Area Telescope (LAT) field of view; however, Mei et al. (2022) reported detection of photons in the GeV range at $\sim T_0 + 10^4$ s. Swift Burst Alert Telescope (BAT) (D’Ai et al. 2021), CALET (Tamura et al. 2021), SPectrometer on

INTEGRAL/Advanced Camera for Surveys (Minaev et al. 2021), and Insight-HXMT (Zhang et al. 2021) also detected GRB 211211A.

The duration $T_{90} = 34.3 \pm 0.6$ s is calculated as the central 90th percentile of the cumulative energy flux in the 50–300 keV range using the `RMfit`¹⁴ software. The hardness ratio over the T_{90} duration, defined as the ratio of fluxes between 50–300 keV and 10–50 keV energy ranges is $HR = 0.850 \pm 0.015$. These two parameters place GRB 211211A on the duration–hardness plane with high probability in the long population (Bhat et al. 2016; von Kienlin et al. 2020; Rouco Escorial et al. 2021; Rastinejad et al. 2022). For spectral analysis we use NaI detectors n2 and na and BGO detector b0. For temporal analysis we can use additional NaI detectors with significant flux: n0, n1, n2, n5, n9, na, and nb.

2.1. Lightcurve

Morphologically, the lightcurve can be separated into three parts. This GRB starts with a brief standalone pulse, a precursor, lasting about 0.2 s. Interestingly, Xiao et al. (2022) reported tentative quasiperiodic oscillations for this pulse. The second part is the brightest, and we refer to it as the *main emission* episode. It starts at $T_0 + 1$ s and lasts until $T_0 + 13$ s. It consists of a large number of short peaks. The third part starts around $T_0 + 13$ s, and we refer to it as *late emission*. It contains less variability than the main emission, it can be detected until about $T_0 + 70$ s, and it fades smoothly into the background (see Figure 1).

Taken by itself, with a duration of ≈ 10 s, even the *main emission* episode would be classified as an IGRB. It is significantly longer than the ≈ 4 –5 s limit separating the short and long classes of GBM (von Kienlin et al. 2020). This limit represents the duration of equal probability between the long and short classes when we model the duration distribution using two log-normal components (see, e.g., Section 4.4 and the associated figure).

¹⁴ <https://fermi.gsfc.nasa.gov/ssc/data/analysis/rmfit>

Table 1
Spectral Parameters of GRB 211211A

Time (s) $T-T_0$ (s)	E_{peak} (keV)	α	β	Energy Flux (10^{-5} erg cm^{-2} s^{-1})	Fluence (10^{-5} erg cm^{-2})	L_{iso} (10^{51} erg s^{-1})	E_{iso} (10^{52} erg)
0–52.2	$545_{-10.8}^{+12.3}$	$-1.180_{-0.006}^{+0.005}$	$-2.13_{-0.019}^{+0.02}$...	50.7 ± 0.1	...	1.25 ± 0.003
7.104–7.168	1737_{-121}^{+114}	$-0.878_{-0.020}^{+0.019}$	$-2.90_{-0.19}^{+0.26}$	14.9 ± 0.2	...	5.89 ± 0.09	...
7.168–8.192	1033_{-31}^{+27}	$-0.941_{-0.008}^{+0.008}$	$-2.72_{-0.06}^{+0.07}$	8.10 ± 0.04	...	2.33 ± 0.01	...

Note. Spectral parameters for GRB 211211A fitting a Band function and using the standard time intervals: the entire GRB, brightest 1024 ms and 64 ms. The flux and fluence are reported in the 10–1000 keV range. L_{iso} and E_{iso} are reported in the 1–10,000 keV (observer) range.

2.2. Spectrum

To compare GRB 211211A with other GRBs, we perform a spectral analysis of the brightest peak and the time-integrated emission. We note that the time-integrated analysis, with fluence $F = (5.1 \pm 0.1) \times 10^{-4}$ erg cm^{-2} , does not capture the evolving trends observed in this burst by, e.g., Gompertz et al. (2023), but it is suitable to determine the gamma-ray energetics. The peak flux, commonly reported on 64 ms (sGRBs) and 1.024 s (IGRBs) timescales, is $P_{64\text{ms}} = (1.49 \pm 0.02) \times 10^{-4}$ erg cm^{-2} s^{-1} and $P_{1\text{s}} = (8.10 \pm 0.04) \times 10^{-5}$ erg cm^{-2} s^{-1} , respectively. Both the time-integrated and the peak spectra are best fit by Band functions (Band et al. 1993) with parameters presented in Table 1.

The redshift reported for the host galaxy is $z = 0.076$ (Malesani et al. 2021), corresponding to a luminosity distance of $D_L = 346$ Mpc (using $\Omega_m = 1 - \Omega_\Lambda = 0.315$ and $H_0 = 67.4$ km s^{-1} Mpc $^{-1}$; Planck Collaboration et al. 2020). The isotropic-equivalent gamma-ray energy of GRB 211211A calculated in the 1–10,000 keV range is $E_{\text{iso}} \approx 1.3 \times 10^{52}$ erg, the peak luminosity, calculated on a 64 ms and 1.024 s timescale is $L_{\text{iso},64\text{ms}} \approx 5.9 \times 10^{51}$ erg s^{-1} and $L_{\text{iso},1\text{s}} \approx 2.3 \times 10^{51}$ erg s^{-1} , respectively (see Table 1).

2.3. GRB 211211A in Context of Other GRBs

GRB 211211A has higher energy fluence (units of erg cm^{-2}) than all but four GRBs in the GBM catalog (GRBs 130427A, 161625B, 171010A and 160821A; von Kienlin et al. 2020), corresponding to the 99.9th percentile among Fermi–GBM GRBs (Poolakkil et al. 2021). The peak energy flux (units of erg cm^{-2} s^{-1}) of GRB 211211A calculated for the brightest 64 ms is brighter than all sGRBs in the catalog. The 1.024 s peak energy flux of GRB 211211A is brighter than all but two IGRBs prior to GRB 211211A (GRB 130427A: Preece et al. 2014; GRB 131014A: Guiriec et al. 2015).

During the writing of this Letter, Fermi–GBM detected GRB 221009A (Lesage et al. 2023) and GRB 230307A (Dalessi & Fermi GBM Team 2023b) with peak fluxes and fluence larger than GRB 211211A. While GRB 221009A is clearly not from a compact binary merger, e.g., because of an underlying supernova detection (Blanchard et al. 2023; Fulton et al. 2023; but see Shrestha et al. 2023), GRB 230307A does bear some resemblance to GRB 211211A (see Section 3.2).

The peak energy (E_{peak}) measured for the brightest 1 s (1030 keV) is the 94.9th percentile among IGRBs and the 84.9th percentile among sGRBs.

We conclude that GRB 211211A is at the bright end of peak flux and fluence distributions among both short and the long classes, making it an exceptional GRB in the Fermi–GBM sample.

3. Minimum Variability Timescale

The minimum variability timescale (MVT; denoted by Δt_{var}) of a GRB lightcurve represents the shortest timescales at which coherent changes can be identified. In practice it coincides with the typical timescale (e.g., the rise time) of the shortest pulse in the lightcurve. There are multiple mathematical methods in the literature to derive the MVT. Here we use the methods of Bhat et al. (2012), Bhat (2013), and Golkhou et al. (2015). Other methods, e.g., MacLachlan et al. (2013), give consistent MVT values when applied to the same GRB.

We binned our lightcurve to 100 μs and searched for the shortest coherent variations. The variability using the method of Bhat et al. (2012) is $\Delta t_{\text{var}} = 2.6 \pm 0.9$ ms. The Golkhou et al. (2015) method gives a variability of $\Delta t_{\text{var}} = 2.5 \pm 0.8$ ms. The two methods are independent, and they give consistent MVT values, strengthening the confidence that this is indeed the minimum variability timescale of this burst.

In addition, we identify a pulse with a rise time of ≈ 2 ms in Figure 1 (inset) that determines the MVT: we fit the high-resolution (400 μs) lightcurve in the range 1.73–1.81 s (region of the lightcurve where the variability time is the shortest) with the pulse model of Norris et al. (2005), using three pulses plus a long-term emission modeled as a first-degree polynomial. The rise time of the shortest pulse is consistent with the minimum variability timescale, as expected (Bhat et al. 2012). This ~ 2 ms timescale is significantly lower than the 16 ms variability reported by Yang et al. (2022) and the 10 ms reported by Xiao et al. (2022). This is possibly due to the fact that these studies related the variability to the shortest Bayesian blocks and did not conduct a dedicated variability search.

We also performed a time-resolved variability analysis. We calculate the MVT in each 1 s bin (Figure 1) and find that the separation of the lightcurve into *main* and *late* emission is also reflected in the evolution of the variability timescale: the main emission episode has a clearly shorter variability than the late emission.

3.1. Long-duration GRBs with Short MVT

GRB 211211A, with an MVT ~ 2.5 ms is a clear outlier in the distribution of the MVTs presented in Golkhou et al. (2015; see Figure 2, where we plot MVT values that have an uncertainty smaller than the value itself). We have searched for other GRBs that have long duration ($T_{90} \gg 2$ s) and short variability. The sample of Golkhou et al. (2015) contained MVT values only until 2012. We extended their sample with bursts up to 2022, with additional 2124 Fermi–GBM GRBs (Table 2).

Because the MVT calculation depends on multiple input parameters that can affect the final value (e.g., detector selection, background, foreground interval, method), we allow

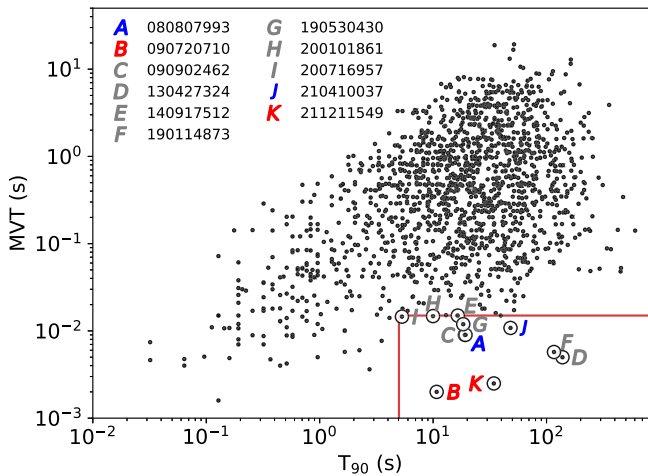


Figure 2. MVT values as a function of T_{90} for all Fermi–GBM GRBs with well-measured T_{90} and MVT. We highlight GRBs with $T_{90} > 5$ s and $MVT < 15$ ms (red line) by displaying the GBM trigger number in the legend. GRB 211211A and GRB 090720B are indicated by red letters (B, K); blue letters (A, J) mark two possibly similar GRBs, but with higher MVT; other selected GRBs have gray letters.

Table 2
Table of MVT Values for GBM GRBs

GRB	T_{90} (s)	MVT (s)
120712571	22.528 ± 5.431	0.6646 ± 0.1799
120716577	24.960 ± 3.958	7.7225 ± 1.8755
120728934	32.768 ± 2.429	1.5558 ± 0.6006
120805706	1.856 ± 1.296	0.6957 ± 0.1710
120806007	26.624 ± 1.557	0.2707 ± 0.1133
120811014	0.448 ± 0.091	0.0182 ± 0.0066

Note. The table contains GRBs starting from the end of GRBs covered in Golkhou et al. (2015).

(This table is available in its entirety in machine-readable form.)

a limit of $MVT < 15$ ms and $T_{90} > 5$ s in searching for GRB similar to GRB 211211A (see Figure 2).

Applying the above limit, we found 10 potentially interesting GRBs in our sample (see Figure 2). Many of the selected bursts are known, bright GRBs with associated supernovae (e.g., GRB 130427A: Preece et al. 2014; GRB 190114C: Ajello et al. 2020), or their lightcurve does not resemble that of GRB 211211A. We inspected each GRB lightcurve visually, looking for similar lightcurve morphology to GRB 211211A, namely, an initial bright, variable phase followed by a longer, less luminous emission episode. After visual inspection of the candidates, we find three additional cases with similar lightcurves as GRB 211211A. Among these three, only GRB 090720B has a comparable variability timescale (~ 2 ms), while other similar GRBs, 210410A and 080807, have ~ 10 ms variability. We thus conclude that bursts with long duration and short variability are rare, especially those GRBs that exhibit a short pulse followed by softer, extended emission. We further conclude that GRB 211211A lies at the extreme low end of the variability timescale distribution of Fermi GRBs.

3.2. Other Examples of Long Duration and Short MVT

GRB 090720B (GBM trigger 090720710; Burgess et al. 2009) was a bright GRB, with similar properties to

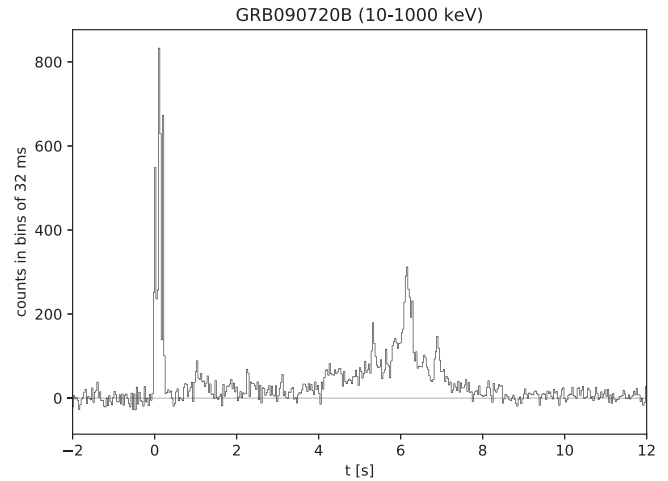


Figure 3. Lightcurve of GRB 090720B with similar short pulse + extended emission structure. GRB 090720B has a similarly short (~ 2 ms) variability timescale as GRB 211211A.

GRB 211211A: an initial bright, highly variable set of overlapping pulses, followed by weaker, less variable emission (Figure 3). We cross-check the short variability measurement by Golkhou et al. (2015), $\Delta t = 2 \pm 1$ ms, and consistently find $\Delta t = 2.6 \pm 0.9$ ms with the method of Bhat et al. (2012). The duration of this GRB is $T_{90} = 10.8 \pm 1.1$ s. Time-resolved variability similarly shows a shorter timescale in the main emission compared to the longer-lasting episode. GRB 090720B has no redshift measurement; however, it is detected by Fermi–LAT (Rubtsov et al. 2012; Ajello et al. 2019).

Two further examples with a larger variability timescale (~ 10 ms) are GRB 080807 (von Kienlin et al. 2020) and 210410A (Wood et al. 2021) with T_{90} of 19.1 ± 0.2 s and 48.1 ± 2.8 s, respectively. Neither have a redshift measurement. Except for GRB 080807, the other three selected GRBs have been detected at high energy by LAT. GRB 080807 occurred in an unfavorable geometry for LAT.

GRB 230307A is a recent bright GRB that has tentatively similar properties to GRB 211211A. Despite its long duration ($T_{90} \approx 35$ s; Dalessi & Fermi GBM Team 2023b) it shows short variations like GRB 211211A and has a tentative kilonova signature (Levan et al. 2023). Because of its extreme brightness the prompt measurement suffers from instrumental effects (Dalessi & Fermi GBM Team 2023a). A detailed study of GRB 230307A is left for a forthcoming paper.

4. Results

4.1. GRB 211211A as a Short GRB with Extended Emission

GRB 060614 (Gehrels et al. 2006), a nearby long event with duration in excess of 100 s, has no supernova detection to deep limits, lag and luminosity consistent with short GRBs, indicating a possible merger origin. Its lightcurve morphology, a short pulse, followed by extended emission established a new category of GRBs (sGRB-EE). GRB 060614 was detected by Swift–BAT. For this GRB we derive an MVT value of $\Delta t_{\text{var}} = 36 \pm 4$ ms. Given that BAT and GBM have different energy ranges we can ask how this value compares with the GBM sample. Golkhou et al. (2015) explored the difference between MVTs measured by BAT and GBM and found good agreement, when the GBM range (8–1000 keV for NaI

Table 3
Sample of Short GRBs with Extended Emission

Trigger Number	MVT (ms)	T_{90} (s)
081110601	291 ± 11	11.8 ± 2.6
090227772	~ 5	1.28 ± 1.03
090510016	5 ± 1	0.96 ± 0.14
090831317	15 ± 4	39.4 ± 0.6
100916779	88 ± 8	12.8 ± 2.1
111221739	18 ± 6	27.1 ± 7.2
140819160	43 ± 20	6.7 ± 3.7
170728961	54 ± 15	46.3 ± 0.8
180618030	~ 7	3.7 ± 0.6
190308923	~ 419	45.6 ± 2.83
200219317	~ 55	1.15 ± 1.03
200313456	~ 284	5.2 ± 4.4
201104001	25 ± 8	52.5 ± 7.4

Note. Values without errors represent cases where the signal to noise was not sufficient to determine an error.

detectors) was restricted to the BAT range (15–350 keV). Variability timescales are shorter with increasing energy in the GBM band, and GBM would have measured a slightly shorter MVT for GRB 060614. Based on the distribution of MVTs with energy in Golkhou et al. (2015), we estimate a discrepancy of $\lesssim 10\%$. Rastinejad et al. (2022), Troja et al. (2022), Xiao et al. (2022), and Gompertz et al. (2023) find that GRB 211211A has broadly consistent properties with other sGRB-EE GRBs. We also find that GRB 211211A has consistent features with sGRB-EE. The time-resolved MVT (Figure 1) also clearly delineates the sGRB and the extended emission.

Kaneko et al. (2015) considered a sample of sGRB-EE in the Fermi–GBM sample. We extend their list (see Table 3) and investigate the variability timescale of sGRB-EE (E. Burns et al. 2023, in preparation). We find that GRB 211211A has a shorter variability timescale than all the GBM sGRB-EE. This means that the MVT of GRB 211211A is extreme also among the sGRBs with extended emission (including the archetypal GRB 060614). We also note that the MVT of GRB 211211A is close to the short end of even the short-duration GRBs (see Figure 2).

4.2. Possible Afterglow Origin of the Late Emission

As noted in the previous section, GRB 211211A fits into the category of sGRB with extended emission (Gehrels et al. 2006; Norris et al. 2010). The main emission plays the role of the short GRB, and the late emission episode corresponds to the extended emission.

The origin of the extended emission is unclear, sometimes it is associated with late energy injection into the GRB (e.g., Bucciantini et al. 2012). In many cases, the extended emission has appreciable variability and for this reason its association with afterglow emission is generally disfavored (Norris & Bonnell 2006). Based on the fact that the late emission (T_0+12 to T_0+70 s in Figure 1) has a longer variability timescale than the main emission, we explore the afterglow origin for the late emission. In this scenario the late emission is emitted by the shocked circumstellar medium as it slows down the shells that were responsible for the prompt emission. Detecting the afterglow in the γ -ray regime has been reported before (e.g.,

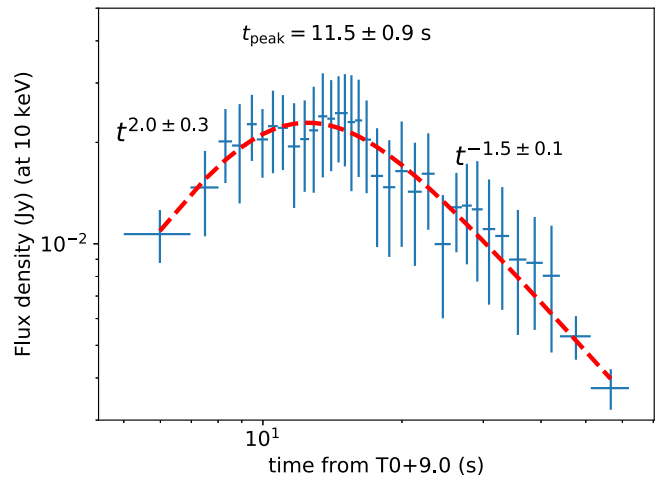


Figure 4. Flux density evolution of the late emission, fit with a smoothly broken power law. The time axis is shifted by 9 s with respect to the trigger time to match the end of the main episode.

Giblin et al. 1999; Connaughton 2002; Ajello et al. 2020), and it is common for bright GRBs.

Early afterglow lightcurves, especially in X-ray and GeV sometimes show a rising phase, a peak, and a decay representing the onset of the afterglow. Here the peak marks the deceleration time. We binned the GBM lightcurve from 13 to 70 s after the trigger into bins with a signal-to-noise ratio of 60. We fit each spectrum with a Comptonized function (power law with exponential cutoff) and calculate the flux density at 10 keV (see Figure 4). The flux evolution shows a clear peak. We fit the flux density curve with a smoothly broken power-law function, $f(t) \propto [(t/t_{\text{peak}})^{s\alpha_{\text{rise}}} + (t/t_{\text{peak}})^{s\alpha_{\text{decay}}}]^{-1/s}$, where s is the smoothness parameter, fixed here to 1. We find the index of the rising phase $\alpha_{\text{rise}} = 2.0 \pm 0.3$ consistent with the expectation of $\alpha_{\text{rise}} = 2$ if it originates from the forward shock before deceleration (Sari & Piran 1999). We note that α_{rise} is sensitive to the choice of the zero-point. Here we choose $T_0 + 9$ s, because this is the approximate end time of the highly variable main emission episode. The peak of the flux occurs at 20.5 ± 0.9 s after the trigger time. The temporal decay index after the peak is $\alpha_{\text{decay}} = -1.5 \pm 0.1$, which in the forward shock scenario corresponds to $1/2 - 3p/4$, where p is the index of shocked electron population’s power-law distribution. In our case we get $p = 2.7 \pm 0.1$, which is consistent with the values that are commonly found for afterglows (e.g., Panaitescu & Kumar 2001).

We thus conclude that the afterglow interpretation is possible at least in some cases of GRBs with extended emission.

4.3. Lorentz Factor Constraints

The Lorentz factor of the outflow is a basic ingredient of the physical picture. We can provide a lower limit on the Lorentz factor if the highly variable prompt gamma-ray lightcurve is produced by internal shocks (Rees & Mészáros 1994). In this scenario the emission radius (R_{IS}) has to be above the photosphere (R_{ph}) where the optical depth is unity. The internal shock radius is $R_{\text{IS}} \approx 2c\Gamma^2\Delta t_{\text{var}}$, while the photosphere radius is $R_{\text{ph}} = L\sigma_T/8\pi m_p c^3\Gamma^3$, assuming the photosphere occurs in the coasting phase (i.e., the jet does not accelerate any more, Γ

(R) = constant). From $R_{\text{IS}} \gtrsim R_{\text{ph}}$, we have

$$\Gamma \gtrsim 170 \left(\frac{L_{\gamma,51.8}}{\eta_{\gamma,-0.7}} \right)^{1/5} \left(\frac{\Delta t_{\text{var}}}{2.5 \text{ ms}} \right)^{-1/5}. \quad (1)$$

A meaningful Lorentz factor constraint using this method is only possible for GRBs with high luminosity and short variability, uniquely relevant for GRB 211211A.

We can calculate the bulk Lorentz factor by identifying the peak of Figure 4 with the onset of the afterglow or the deceleration time. The deceleration radius corresponding to the deceleration time (t_{dec}) marks the distance from the central engine where the relativistic outflow has plowed up interstellar matter that is a fraction $\sim 1/\Gamma$ of the jet mass. Using the expression of t_{dec} , the Lorentz factor evolving a constant-density medium will be

$$\Gamma = \left(\frac{3E_k}{4\pi m_p c^5 n} \right)^{1/8} t_{\text{dec}}^{-3/8} \quad (2)$$

$$\approx 1200 \left(\frac{E_{\gamma,52.1}}{n_{-4} \eta_{\gamma,-0.7}} \right)^{1/8} \left(\frac{t_{\text{peak}}}{11.5 \text{ s}} \right)^{-3/8}. \quad (3)$$

Here we chose a gamma-ray efficiency of $\eta_{\gamma} = E_{\gamma}/E_k = 7.8\%$, where E_k is the kinetic isotropic-equivalent energy and $n = 10^{-4} \text{ cm}^{-3}$ is the constant interstellar number density, as scaling values, from Mei et al. (2022). If we conservatively measure the peak from the trigger time, instead of the 9 s shift that we introduced, the Lorentz factor becomes $\Gamma \approx 980$.

Sonbas et al. (2015) present a correlation between variability timescale and Lorentz factor based on a compilation of Lorentz factor estimates. The relationship they find is $t_{\text{var}}(\Gamma) \propto \Gamma^{-4}$ for $\Gamma \gtrsim 200$ and $t_{\text{var}} \approx \text{constant}$ otherwise. Inverting the correlation, and substituting $\Delta t_{\text{var}} = 2.5 \text{ ms}$, we get $\Gamma \approx 900$, which is consistent with the above estimates. Furthermore, the Lorentz factor estimates from different methods are consistent with the best estimate by Mei et al. (2022) of $\log \Gamma \approx 3.1_{-0.6}^{+0.9}$. In the internal shock scenario the emission radius of the gamma-rays will be

$$R_{\gamma} \approx 2\Gamma^2 c \Delta t_{\text{var}} = 1.5 \times 10^{14} \Gamma_3^2 \left(\frac{\Delta t_{\text{var}}}{2.5 \text{ ms}} \right) \text{ cm}. \quad (4)$$

Lorentz factor values determined from, e.g., the peak of the afterglow are in the few hundreds, depending on the assumed density profile. For example, Ghirlanda et al. (2018) report a range of 200–700 for a particular set of assumptions. Brighter GRBs like GRB 211211A, albeit with prompt GeV observations, can have inferred Lorentz factors in excess of 1000, based on pair opacity arguments (Abdo 2009; Ackermann & the Fermi collab 2010).

4.4. Event Rate: The Tail of the Merger Distribution

The 10 yr GBM GRB catalog (von Kienlin et al. 2020) contains in excess of 2300 GRBs with duration measurements. The distribution of the T_{90} durations is modeled as the sum of two log-normal functions (merger-origin or short component and massive-star-origin or long component). The exact reason why the T_{90} distribution would follow a log-normal distribution is unclear (for a possible explanation, see Ioka & Nakamura 2002), and in reality the distributions could be asymmetrical (Tarnopolski 2019; see Dimple & Arun 2023 for

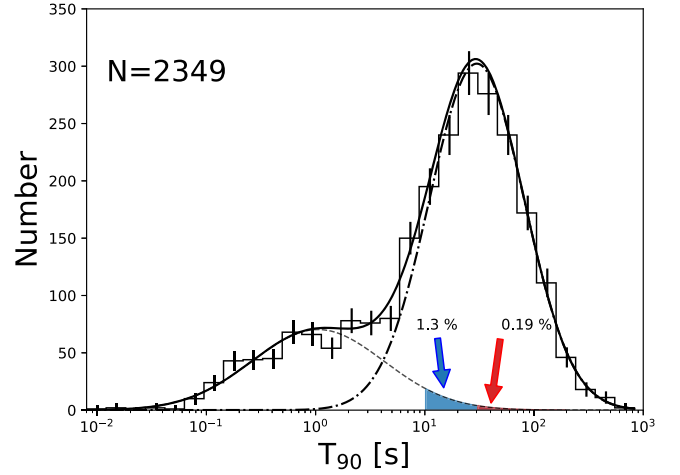


Figure 5. T_{90} distribution of 10 yr of GBM GRBs (von Kienlin et al. 2020). Fractions of short GRBs with $T_{90} > 10 \text{ s}$ and $T_{90} > 30 \text{ s}$ are indicated.

a classification based on machine learning). Because the two-component model provides a good fit to the distribution, we will consider this description to calculate the rate for mergers masquerading as IGRBs (see Figure 5).

We integrate the merger-origin (peaking around 1 s) model from 10 s, broadly corresponding to the duration of the main emission and the actual $T_{90} \sim 10 \text{ s}$ of the similarly short MVT GRB 090720B (Section 3.2). We also integrate the merger-origin model component for $T_{90} > 30 \text{ s}$ corresponding roughly to the T_{90} of GRB 211211A. We find about 1.3 % (3 per year) of merger-origin Fermi–GBM GRBs will have $T_{90} > 10 \text{ s}$ and about 0.19 % (0.4 per year) of merger-origin GRBs will have $T_{90} > 30 \text{ s}$.

4.5. Implications for Searches for GW Counterparts

Having characterized the gamma-ray emission of GRB 211211A, there still remains an intriguing question. How can a merger event give rise to a GRB that has a duration well in excess of the historical 2 s limit between the short and long classes? Lu & Quataert (2023), for example, ascribe the extended emission to the long-term evolution of the accretion disk after the merger, and Metzger et al. (2008) invoke the spindown power of a protomagnetar for the extended emission. Even if we place GRB 211211A at a larger distance where only the main emission episode is detectable, its duration will be $\sim 10 \text{ s}$ and it will be classified as a likely IGRB. This suggests that GRBs with duration $\gtrsim 5 \text{ s}$ can possibly originate from compact binary mergers and be GW counterparts. Follow-up decisions should consider this fact.

If a subclass of IGRBs corresponds to compact binary mergers as their source then this will have implications for the gravitational-wave signal search strategy of LIGO–Virgo–KAGRA (LVK). Currently LVK search for gravitational waves in coincidence with GRBs detected by the Fermi and Swift satellites (Abbott et al. 2021, 2022; see also Wang et al. 2022). In these searches, GRBs are classified as short if $T_{90} < 2 \text{ s}$, long if $T_{90} > 4 \text{ s}$, or ambiguous for all the other cases. The times coincident with GRBs classified as short or ambiguous are searched for GW signals from compact binary mergers using a coherent matched filter analysis, PyGRB (Harry & Fairhurst 2011; Williamson et al. 2014). The merger time is assumed to fall within a $[-5, 1] \text{ s}$ window, where 0 corresponds to the GRB trigger time.

LVK also use an excess power analysis to search for generic transient signals associated with all GRBs, namely, X-Pipeline (Sutton et al. 2010; Was et al. 2012). The search window for GW transients begins 600 s before the GRB trigger time and stops 60 s after trigger time; if $T_{90} > 60$ s then the end of the search window is T_{90} .

During observing run O3, times coincident with 49 GRBs were examined targeting compact binary merger signals. The times coincident with 191 GRBs were examined with the generic search pipeline (Abbott et al. 2021, 2022). If only the GRB T_{90} is considered, as is presently the case for these LVK analyses, then including GRBs such as GRB 211211A will require a significant broadening of the “ambiguous” class, considerably increasing the number of GRBs that will have to be analyzed with the compact binary merger pipeline. This is not an impossible challenge, but would require significantly more human and computing resources, and would increase the chance of a false alarm from the significantly larger sample of GRBs that are not originated by compact binary mergers.

The results of this study motivate the design of a more reliable GRB classification scheme that includes the MVT in addition to T_{90} . The observation of a kilonova should obviously also be incorporated into this improved classification.

5. Discussion and Conclusion

The observation of GRB 211211A represents one of the clearest examples that defy the duration based GRB classification scheme. We analyzed the gamma-ray properties of GRB 211211A in context of the Fermi–GBM GRB population. We found that GRB 211211A is one of the brightest GRBs among both the merger and collapsar populations.

We found indications that the extended emission can be modeled as early afterglow in the gamma-rays, and that leads to an estimate of the Lorentz factor. We calculated the variability timescale with different methods and conclusively found one of the shortest variations among long-duration GRBs. The short variability has implications on the emission mechanisms and lets us determine the physical parameters of the source. We found the Lorentz factor consistent with $\Gamma \approx 1000$, which puts it among the highest inferred values. $\Gamma \approx 1000$ agrees well with the value reported by Mei et al. (2022), and it is larger than the values (≈ 100) derived by Rastinejad et al. (2022) and Gompertz et al. (2023).


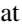

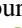



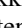
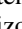
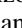


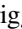





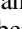
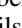


We estimated the fraction of sGRBs based on the best fit to the duration distribution. Even though the extrapolation is uncertain, we can conclude that ~ 3.1 GRBs per year with merger origin will have $T_{90} > 10$ s and 0.44 GRBs per year will have $T_{90} > 30$ s.

The realization that IGRBs can also emanate from binary mergers has profound implications on the follow-up program of future GW observations. First of all, if a GRB presents a spike and extended emission structure, follow-up is warranted. Here we propose that fast variations in the lightcurve may be a distinguishing feature of mergers. It is more likely, however, that the variations have a continuous distribution and GRB 211211A is special even among the short GRBs with extended emission. Indeed, we found that only one IGRB has comparably short MVT. The flux and fluence of GRB 211211A are both extreme among the Fermi–GBM GRBs.

Acknowledgments

We thank the anonymous referee for a prompt and insightful report. UAH coauthors acknowledge NASA funding from cooperative agreement 80MSFC22M0004. N.F. is grateful to UNAM-DGAPA-PAPIIT for the funding provided by grant IN106521. USRA coauthors acknowledge NASA funding from cooperative agreement 80MSFC17M0022. R.H. acknowledges funding from the European Union’s Horizon 2020 research and innovation program under the Marie Skłodowska-Curie grant agreement No. 945298-ParisRegionFP.

ORCID iDs

P. Veres  <https://orcid.org/0000-0002-2149-9846>
 P. N. Bhat  <https://orcid.org/0000-0001-7916-2923>
 E. Burns  <https://orcid.org/0000-0002-2942-3379>
 R. Hamburg  <https://orcid.org/0000-0003-0761-6388>
 N. Fraija  <https://orcid.org/0000-0002-0173-6453>
 D. Kocevski  <https://orcid.org/0000-0001-9201-4706>
 R. Preece  <https://orcid.org/0000-0003-1626-7335>
 S. Poolakkil  <https://orcid.org/0000-0002-6269-0452>
 N. Christensen  <https://orcid.org/0000-0002-6870-4202>
 M. A. Bizouard  <https://orcid.org/0000-0002-4618-1674>
 T. Dal Canton  <https://orcid.org/0000-0001-5078-9044>
 S. Bala  <https://orcid.org/0000-0002-6657-9022>
 E. Bissaldi  <https://orcid.org/0000-0001-9935-8106>
 M. S. Briggs  <https://orcid.org/0000-0003-2105-7711>
 W. Cleveland  <https://orcid.org/0009-0003-3480-8251>
 A. Goldstein  <https://orcid.org/0000-0002-0587-7042>
 B. A. Hristov  <https://orcid.org/0000-0001-9556-7576>
 C. M. Hui  <https://orcid.org/0000-0002-0468-6025>
 S. Lesage  <https://orcid.org/0000-0001-8058-9684>
 B. Mailyan  <https://orcid.org/0000-0002-2531-3703>
 O. J. Roberts  <https://orcid.org/0000-0002-7150-9061>
 C. A. Wilson-Hodge  <https://orcid.org/0000-0002-8585-0084>

References

- Abbott, B. P., Abbott, R., Abbott, T. D., et al. 2017, *ApJL*, 848, L13
 Abbott, R., Abbott, T. D., Abraham, S., et al. 2021, *ApL*, 915, 86
 Abbott, R., Abbott, T. D., Acernese, F., et al. 2022, *ApL*, 928, 186
 Abdo, A. A., Ackermann, M., Ajello, M., et al. 2009, *ApJL*, 706, L138
 Ackermann, M., Asano, K. & The Fermi Collaboration 2010, *ApJ*, 716, 1178
 Ajello, M., Arimoto, M., Axelsson, M., et al. 2019, *ApJ*, 878, 52
 Ajello, M., Arimoto, M., Axelsson, M., et al. 2020, *ApJ*, 890, 9
 Band, D., Mateson, J., Ford, L., et al. 1993, *ApJ*, 413, 281
 Bhat, N. P., Meegan, C. A., von Kienlin, A., et al. 2016, *ApJS*, 223, 28
 Bhat, P. N. 2013, arXiv:1307.7618
 Bhat, P. N., Briggs, M. S., Connaughton, V., et al. 2012, *ApJ*, 744, 141
 Bhat, P. N., Fishman, G. J., Meegan, C. A., et al. 1992, *Natur*, 359, 217
 Blanchard, P. K., Villar, V. A., Chornock, R., et al. 2023, *GCN*, 33676, 1
 Bucciantini, N., Metzger, B. D., Thompson, T. A., & Quataert, E. 2012, *MNRAS*, 419, 1537
 Burgess, J. M., Goldstein, A., & van der Horst, A. J. 2009, *GCN*, 9698, 1
 Burns, E., Svinkin, D., Hurley, K., et al. 2021, *ApJL*, 907, L28
 Camisasca, A. E., Guidorzi, C., Amati, L., et al. 2023, *A&A*, 671, A112
 Connaughton, V. 2002, *ApJ*, 567, 1028
 D’Ai, A., Ambrosi, E., D’Elia, V., et al. 2021, *GCN*, 31202, 1
 Dalessi, S. & Fermi GBM Team 2023a, *GCN*, 33551, 1
 Dalessi, S. & Fermi GBM Team 2023b, *GCN*, 33407, 1
 Dimple, M. K., & Arun, K. G. 2023, *ApJL*, 949, L22
 Duncan, R. C., & Thompson, C. 1992, *ApJL*, 392, L9
 Fulton, M. D., Smartt, S. J., Rhodes, L., et al. 2023, *ApJL*, 946, L22
 Gehrels, N., Norris, J. P., Barthelmy, S. D., et al. 2006, *Natur*, 444, 1044
 Gendre, B., Stratta, G., Atteia, J. L., et al. 2013, *ApJ*, 766, 30
 Ghirlanda, G., Nappo, F., Ghisellini, G., et al. 2018, *A&A*, 609, A112
 Gibling, T. W., van Paradijs, J., Kouveliotou, C., et al. 1999, *ApJL*, 524, L47

- Goldstein, A., Veres, P., Burns, E., et al. 2017, *ApJL*, 848, L14
- Golkhou, V. Z., Butler, N. R., & Littlejohns, O. M. 2015, *ApJ*, 811, 93
- Gompertz, B. P., Ravasio, M. E., Nicholl, M., et al. 2023, *NatAs*, 7, 67
- Greiner, J., Mazzali, P. A., Kann, D. A., et al. 2015, *Natur*, 523, 189
- Guiriec, S., Mochkovitch, R., Piran, T., et al. 2015, *ApJ*, 814, 10
- Harry, I. W., & Fairhurst, S. 2011, *PhRvD*, 83, 084002
- Hjorth, J., Sollerman, J., Møller, P., et al. 2003, *Natur*, 423, 847
- Ioka, K., & Nakamura, T. 2002, *ApJL*, 570, L21
- Kaneko, Y., Bostanci, Z. F., Göğüş, E., & Lin, L. 2015, *MNRAS*, 452, 824
- Kann, D. A., Klose, S., Zhang, B., et al. 2011, *ApJ*, 734, 96
- Kann, D. A., Schady, P., Olivares, E. F., et al. 2018, *A&A*, 617, A122
- Kouveliotou, C., Meegan, C. A., Fishman, G. J., et al. 1993, *ApJL*, 413, L101
- Lesage, S., Veres, P., Briggs, M. S., et al. 2023, *ApJ*, 952, L42
- Levan, A. J., Gompertz, B. P., Malesani, D. B., et al. 2023, *GCN*, 33569, 1
- Levan, A. J., Tanvir, N. R., Starling, R. L. C., et al. 2014, *ApJ*, 781, 13
- Lien, A., Sakamoto, T., Barthelmy, S. D., et al. 2016, *ApJ*, 829, 7
- Lu, W., & Quataert, E. 2023, *MNRAS*, 522, 5848
- MacFadyen, A. I., & Woosley, S. E. 1999, *ApJ*, 524, 262
- MacLachlan, G. A., Shenoy, A., Sonbas, E., et al. 2013, *MNRAS*, 432, 857
- Malesani, D. B., Fynbo, J. P. U., de Ugarte Postigo, A., et al. 2021, *GCN*, 31221, 1
- Mangan, J., Dunwoody, R., Meegan, C. & Fermi GBM Team 2021, *GCN*, 31210, 1
- Meegan, C., Lichti, G., Bhat, P. N., et al. 2009, *ApJ*, 702, 791
- Mei, A., Banerjee, B., Oganessian, G., et al. 2022, *Natur*, 612, 236
- Metzger, B. D., Quataert, E., & Thompson, T. A. 2008, *MNRAS*, 385, 1455
- Minaev, P., Pozanenko, A., & IKI, G. R. B. 2021, *GCN*, 31230, 1
- Morsony, B. J., Lazzati, D., & Begelman, M. C. 2010, *ApJ*, 723, 267
- Narayan, R., & Kumar, P. 2009, *MNRAS*, 394, L117
- Narayan, R., Paczynski, B., & Piran, T. 1992, *ApJL*, 395, L83
- Norris, J. P., & Bonnell, J. T. 2006, *ApJ*, 643, 266
- Norris, J. P., Bonnell, J. T., Kazanas, D., et al. 2005, *ApJ*, 627, 324
- Norris, J. P., Gehrels, N., & Scargle, J. D. 2010, *ApJ*, 717, 411
- Paciesas, W. S., Meegan, C. A., Pendleton, G. N., et al. 1999, *ApJS*, 122, 465
- Paczynski, B. 1998, *ApJL*, 494, L45
- Panaiteanu, A., & Kumar, P. 2001, *ApJL*, 560, L49
- Piro, L., Troja, E., Gendre, B., et al. 2014, *ApJL*, 790, L15
- Planck Collaboration, Aghanim, N., Akrami, Y., et al. 2020, *A&A*, 641, A6
- Poolakkil, S., Preece, R., Fletcher, C., et al. 2021, *ApJ*, 913, 60
- Preece, R., Burgess, J. M., von Kienlin, A., et al. 2014, *Sci*, 343, 51
- Rastinejad, J. C., Gompertz, B. P., Levan, A. J., et al. 2022, *Natur*, 612, 223
- Rees, M. J., & Mészáros, P. 1994, *ApJL*, 430, L93
- Roberts, O. J., Veres, P., Baring, M. G., et al. 2021, *Natur*, 589, 207
- Rouco Escorial, A., Fong, W., Veres, P., et al. 2021, *ApJ*, 912, 95
- Rubtsov, G. I., Pshirkov, M. S., & Tinyakov, P. G. 2012, *MNRAS*, 421, L14
- Rybicki, G. B., & Lightman, A. P. 1979, *Radiative Processes in Astrophysics* (New York: Wiley-Interscience), 393
- Sari, R., & Piran, T. 1997a, *MNRAS*, 287, 110
- Sari, R., & Piran, T. 1997b, *ApJ*, 485, 270
- Sari, R., & Piran, T. 1999, *ApJ*, 520, 641
- Shrestha, M., Sand, D. J., Alexander, K. D., et al. 2023, *ApJL*, 946, L25
- Sonbas, E., MacLachlan, G. A., Dhuga, K. S., et al. 2015, *ApJ*, 805, 86
- Sutton, P. J., et al. 2010, *NJPh*, 12, 053034
- Tamura, T., Yoshida, A., Sakamoto, T., et al. 2021, *GCN*, 31226, 1
- Tarnopolski, M. 2019, *ApJ*, 870, 105
- Thompson, C. 1994, *MNRAS*, 270, 480
- Troja, E., Fryer, C. L., O'Connor, B., et al. 2022, *Natur*, 612, 228
- Usov, V. V. 1992, *Natur*, 357, 472
- von Kienlin, A., Meegan, C. A., Paciesas, W. S., et al. 2020, *ApJ*, 893, 46
- Wang, Y.-F., Nitz, A. H., Capano, C. D., et al. 2022, *ApJL*, 939, L14
- Was, M., Sutton, P. J., Jones, G., & Leonor, I. 2012, *PhRvD*, 86, 022003
- Williamson, A. R., Biwer, C., Fairhurst, S., et al. 2014, *PhRvD*, 90, 122004
- Wood, J., Meegan, C. & Fermi GBM Team 2021, *GCN*, 29788, 1
- Woosley, S. E. 1993, *ApJ*, 405, 273
- Woosley, S. E., & Bloom, J. S. 2006, *ARA&A*, 44, 507
- Xiao, S., Zhang, Y.-Q., Zhu, Z.-P., et al. 2022, arXiv:2205.02186
- Yang, J., Zhang, B. B., Ai, S. K., et al. 2022, *Natur*, 612, 232
- Zhang, B., Zhang, B.-B., Virgili, F. J., et al. 2009, *ApJ*, 703, 1696
- Zhang, Y. Q., Xiong, S. L., Li, X. B., et al. 2021, *GCN*, 31236, 1